The iodine Satellite (iSat) Propellant Feed System - Design and Development

IEPC-2017-11

Kurt A. Polzin,[a] Joao F. Seixal,[b] Stephanie L. Mauro,[c] Adam O. Burt,[d]
Armando Martinez,[e] Adam K. Martin[f]
NASA-George C. Marshall Space Flight Center, Huntsville, AL 35812, USA

The development, modeling, and testing of components and subsystems required to feed iodine propellant to a 200-W Hall thruster and cathode are described. This work aims to address design deficiencies and issues associated with the propellant feed system that were revealed by an integrated thruster-cathode-feed system test. The feed system design is modified to use materials that are more resistant to the highly-reactive nature of iodine propellant. Dynamic modeling indicates that the inclusion of additional constraints on feed system tubing will reduce the vibrationally-induced stresses that occur during launch. Full spacecraft thermal modeling show that the feed system heater power levels are sufficient to heat the tank and propellant lines to operating temperatures, where iodine in the tank is sublimed to supply propellant for operation and the tubing is elevated in temperature to keep propellant from redepositing to block the flow. Experiments are conducted to demonstrate that is it possible through the application of heating to clear an iodine deposit blocking the flow. Deposits in the low-pressure portion of the system near the exit to vacuum are shown to be relatively easy to remove in this manner while blockages forming upstream nearer to the higher-pressure propellant tank require significantly more effort to remove. Fluid flow modeling of the feed system is performed, exhibiting some qualitative agreement with experimental data. However, the highly viscous nature of the fluid flow and the dependence of the component flow coefficients on the Reynolds number are likely causes of the generally-poor quantitative agreement between the modeling results and experimentally-measured fluid flow properties.

I.   Introduction

CUBESATS are relatively new spacecraft platforms that are typically deployed from a launch vehicle as a secondary payload,[1] providing low-cost access to space for a wide range of end-users. These satellites are comprised of building blocks having dimensions of 10x10x10 cm^3 and a mass of 1.33 kg (a 1-U size). While providing low-cost access to space, a major operational limitation is the lack of a propulsion system that can fit within a CubeSat and is capable of executing high Δv maneuvers. This makes it difficult to use CubeSats on missions requiring certain types of maneuvers (i.e. formation flying, spacecraft rendezvous).

While electric thrusters typically provide high specific impulse, there are several challenges associated with the integration of an electric propulsion system into a CubeSat platform. Work has been performed investigating the use of iodine as a propellant for Hall-effect thrusters (HETs)[2] that could subsequently be used to provide a high specific impulse path for CubeSat propulsion,[3] resulting in enough propulsive utility to enable various missions of interest. One of the systems required to support such a technology is the

[a]iSAT Feed System Development Lead, Propulsion Research and Technology Applications Branch, kurt.a.polzin@nasa.gov.
[b]Aerospace Engineer, Structural and Mechanical Design Branch.
[c]Thermal Engineer, Thermal and Mechanical Analysis Branch.
[d]Structural Dynamics Engineer, Thermal and Mechanical Analysis Branch.
[e]Aerospace Engineer, Structural and Mechanical Design Branch.
[f]Physicist, Propulsion Research and Technology Applications Branch.

propellant feed system, which must be capable of storing solid iodine propellant, applying heat to sublime the stored solid into the vapor phase, and then controlling the flow of low-pressure gaseous iodine to both the thruster and cathode. In a test conducted in 2016, a first-generation iodine propellant feed system was integrated with a cathode and Hall thruster.[4] While this test had to be terminated, the feed system in this first test was able to support both cathode and integrated cathode and thruster operation prior to the termination of the test.

In the present paper, we describe work performed since that initial integrated test. The effort uses lessons learned from the previous integrated test, retiring risk associated with the iodine propellant feed system and answering open design-space questions. The work is undertaken at both the component level and then at the integrated subsystem level to systematically improve the feed system design, increasing the hardware fidelity so the appearance and operation of the system are closer to a flight-like level.

The outline for the remainder of this paper is as follows. In Sect. II we present results of the first integrated test, noting specifically the lessons learned regarding the propellant feed system. The feed system design and specifications are described in Sect. III. Results of dynamic analysis of the system are given in Sect. IV, while the results of system-level thermal modeling are presented in Sect. V. In Sect. VI we describe testing undertaken to demonstrate that iodine clogs that might form within the feed system could be subsequently cleared through the application of heat. Finally, feed system flow modeling is presented in Sect. VII.

II.   First Integrated Test Results

An integrated test of the propulsion system was conducted in the summer of 2016. This was the first time that the propellant feed system, thruster, and cathode were operated as a single, complete system. The testing enjoyed some successes, but it also encountered some challenges that ended the testing very early and indicated that further development work and system risk reduction efforts were needed. We discuss herein the results of that test, focusing on the successes and issues directly associated with the propellant feed system.

The propellant feed system was assembled such that the thruster and cathode flows were supplied from a single, common tank but were independently controlled by two first generation proportional flow control valves (PFCVs). For a short time the PFCVs were successful in controlling the iodine flow. More importantly, the cathode and thruster were successfully operated in this configuration. This was, to our knowledge, the first time where a common iodine propellant tank was used to feed simultaneous operation of a Hall thruster and cathode, demonstrating that the feed system design was capable of supplying the requisite flow to operate both devices. In testing, we also demonstrated very stable PID-loop control of the tank, propellant line and PFCV temperatures. This control was achieved by adjusting the duty-cycle on the heaters to maintain a set temperature, which could be adjusted through a user interface during the testing.

During the testing, two specific feed system-related issues arose. A combination of high thermal inertia at the propellant tank exit and a lower-than-required level of heating resulted in a cooler spot at that location. The result of this was a propellant-line clog at the tank exit, which blocked iodine flow and prematurely ended the test. In addition, the PFCVs lost control authority during testing owing to corrosion of the body materials, which resulted in corrosion-product particulates depositing on the sealing surfaces. The former issue indicated that more study was required regarding the thermal design of the feed system and the formation and removal of iodine deposits in the system. The latter issue indicated an problem with the materials of the PFCV and necessitated a reworking of the design to remove the corroding materials.

III.   Feed System Overview and Specifications

The full iSAT propulsion system was described in significant detail in Ref. [5], and will only be briefly reviewed in this paper. The primary components of the iodine Hall thruster propulsion system are labeled in Figs. 1 and 2. Most of the propulsion system components are mounted to a plate and face the aft-end of the spacecraft, external to an enclosure containing the remaining spacecraft components. During operation, the propellant tank and lines are heated to their respective operating temperatures. Iodine is sublimed in the propellant tank the flow out of the tank is split, allowing for a common propellant tank that feeds gaseous iodine to both the cathode and anode. The flow in each branch is controlled using a proportional flow control valve (PFCV). Power for operation of the thruster and cathode, as well as feed system control

functionality, are provided by the power processing unit (PPU). The thruster, a Busek BHT-200-I (a version of the BHT-200 HET that has been modified for compatibility with iodine propellant) has a performance of 1350 s anode I_{sp}, 13.5 mN thrust, 200 W input power ($\sim$1.02 mg/s anode flow rate with an assumed 0.5 mg/s cathode flow rate)
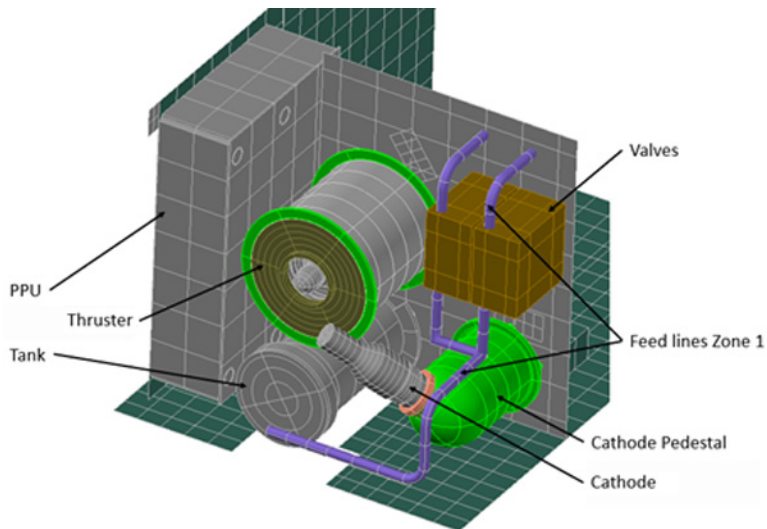

Figure 1. Rendering of Propulsion System Components Viewed from Outside the Chassis.
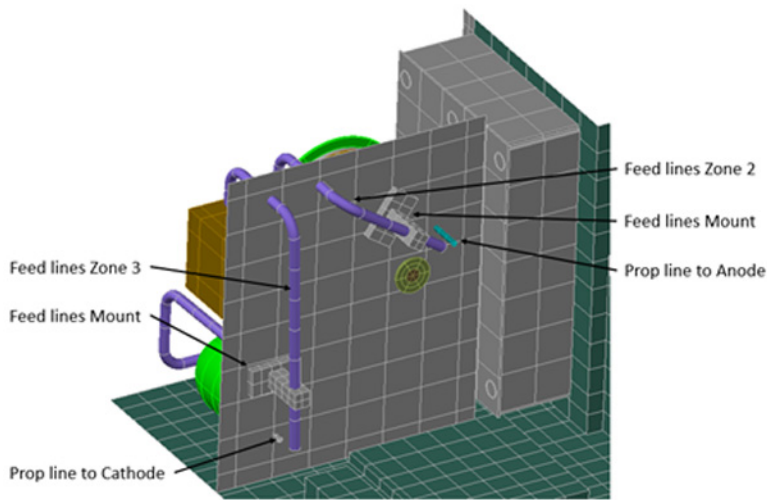

Figure 2. Rendering of Propulsion System Components Viewed from Inside Chassis.

The iSAT mission has several requirements related to the iSAT propellant feed system. Specific ones that guided the design of the system were

- A mission success criteria consisting of 100 thruster operation cycles, with each cycle nominally lasting 300 s (5 mins).

- An iSAT tank volume of $\geq$165 cc (assuming a 20% ullage volume).

- A propellant mass in the iSAT tank of $\geq$370 g iodine.

- During heating and thruster operation, the temperature of the propellant lines and valves, when exposed to iodine vapor, shall always be greater than the temperature of the propellant tank.

    - The temperature of the tank is maintained to a minimum of 90°C during thruster operation.

– The temperature of the propellant feed lines is maintained to a minimum of 120°C during thruster operation.

- The feed system is designed to remain in storage for up to a year before flight.

The propellant tank size and propellant mass are selected to provide a significant margin on the amount of propellant required to achieve the primary mission success criteria.

The PFCVs were redesigned by VACCO, Inc. to address the corrosion and loss of control authority experienced in the first integrated test. The redesign addressed iodine compatibility issues and reduced the thermal mass of the wetted portion of the valve. The wetted valve bodies were changed to hastelloy (as compared to anodized aluminum in the previous valves) and an Inconel screen was incorporated into the design on the inlet to catch debris that might attempt to enter the valve. The reduced thermal mass minimizes the amount of heating required for the valves, and a bellows design is employed to minimize the hysteresis in valve operation making it more repeatable.

IV.   Dynamic Analysis

The purpose of this analysis was to predict the dynamic response of iSAT feed system when undergoing qualification random vibration testing. The current qualification environments are obtained from Ref. [6], Table 2.4-3, which is repeated in Table 1. This table is used in lieu of launch vehicle specific random vibration environments, as at the time of analysis launch environments were not known.

Table 1.   Generalized Random Vibration Environment.[6]

Frequency (Hz)	Generalized Random Vibration Environment 22.7 kg (50 lb) or less (g^2/Hz)	
	Qualification	Acceptance
20	0.026	0.013
50	0.16	0.08
800	0.16	0.08
2000	0.026	0.013
G_{RMS}	14.1	10.0

A finite element model was used to predict the dynamic response of the feed system. This model included a detailed representation of the iodine propellant tank and feed lines. All other components were modeled as point masses with rigid attachments to the support plate. The model boundary conditions assumed that the propulsion mounting plate was hard mounted to a vibration test fixture with infinite stiffness. To match the flight configuration to the best extent possible, a free edge was retained to capture relevant dynamic effects. A view of the finite element model and boundary conditions are presented in Fig. 3.
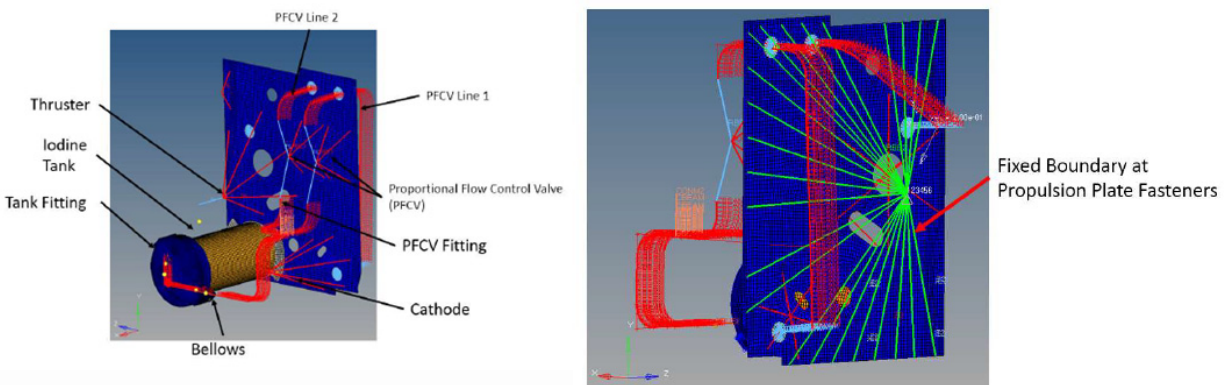

Figure 3.   (left) Feed system finite element model. (right) Feed system plate boundary conditions.

Random Frequency Response analysis was conducted using the modal method available in MSC NAS-TRAN 2017. A flat damping schedule of 1% for every mode was assumed. This assumption is conservative

in light of the lack of test data. Results of the analysis revealed the feed lines, as designed, were inadequately constrained to the plate. A contour plot of the 3σ RMS stress for each element was developed using the random toolbox in MSC PATRAN 2017. The stress results and specific mode shape at 450 Hz as presented in Fig. 4 indicate elements that had stress levels with negative margins of safety. Specifically, the peak stress occurs at the fitting that transitions the tubing from 0.25-in diameter to 0.125-in diameter.
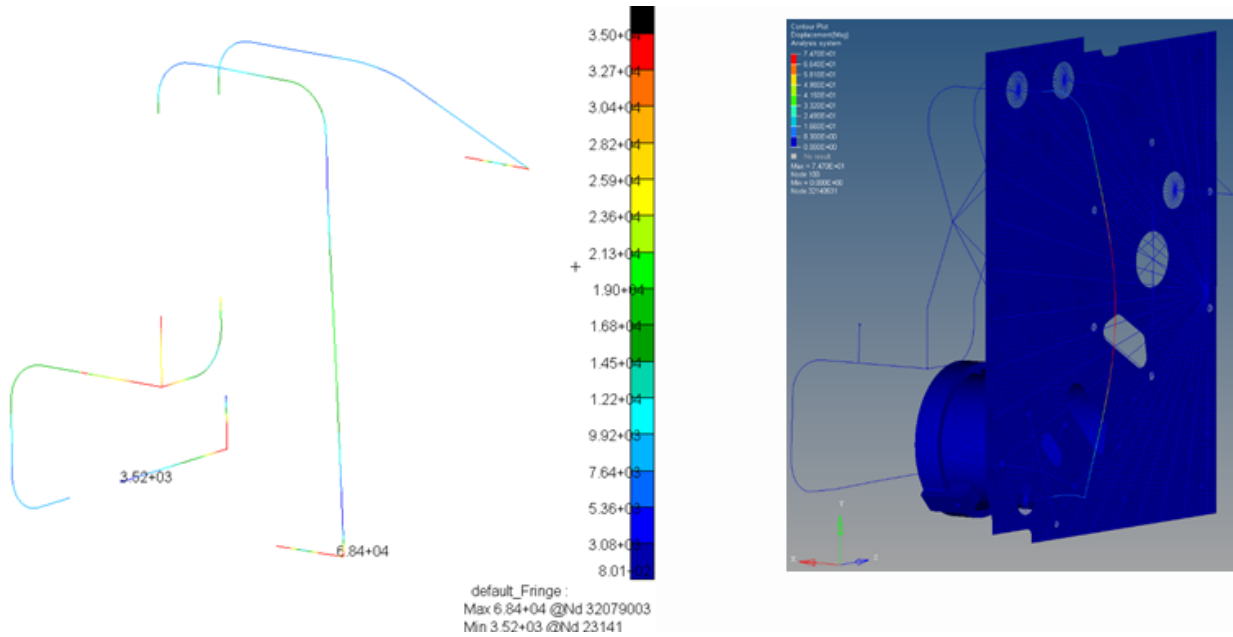

Figure 4. (left) 3σ stress due to x-direction input. (right) Vibrational mode at 450 Hz.

Stress spectral density and cumulative RMS plots (see Fig. 5 were used to determine the mode with highest contribution to the overall stress. This revealed that modes between 400Hz and 500Hz were the greatest contributors to the overall stress and indicated that changes were required to reduce the stresses. Using the modeling results, an optimal clamping location was determined for the PFCV lines on the back side of the propulsion plate. The response of the system with these tubing constraints, also show in the graphs, exhibit a positive margin of safety. It should be noted that for the present situation a typical approach using Miles equation[7] would not have revealed the correct way to support the structure as the high stress case arose due to a higher-order vibrational mode.
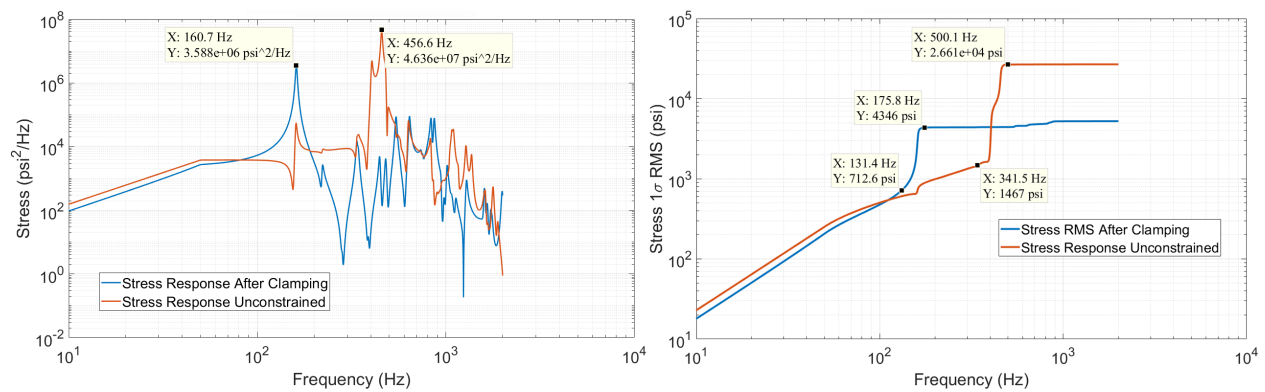

Figure 5. Effect of clamping on (left) stress spectral density and (right) RMS stress.

V. Thermal Modeling

The design of the propellant storage and feeding system for iodine propellant has several unique challenges. The heating system to sublime the iodine and keep it from redepositing must draw a minimal amount of power from the spacecraft while still fulfilling the mission's operational requirements. The present section briefly describes thermal modeling of the integrated propulsion system that was performed to aid in determining the feed system heater requirements for the iSAT mission.

A. Thermal Model

The thermal model was created in Thermal Desktop (Version 5.8 Patch 12) and analyzed with SINDA/FLUINT (Version 5.5 Patch 11). The system thermal model of the iSAT spacecraft, shown in Fig. 6, includes all powered components inside and outside of the chassis, including the propulsion system. The high-fidelity propulsion system model (produced by James Myers, NASA-Glenn Research Center) includes the thruster, cathode and cathode pedestal, PPU, loaded propellant tank, propellant feed lines and mounts, and cathode pedestal (as previously presented in Figs. 1 and 2). All modeling was completed based on beginning of life propellant load of a 700 g of solid, cylindrical iodine.[a] The iodine is loaded as if it was being pressed down with the spring-loaded plate, as it would be in flight.
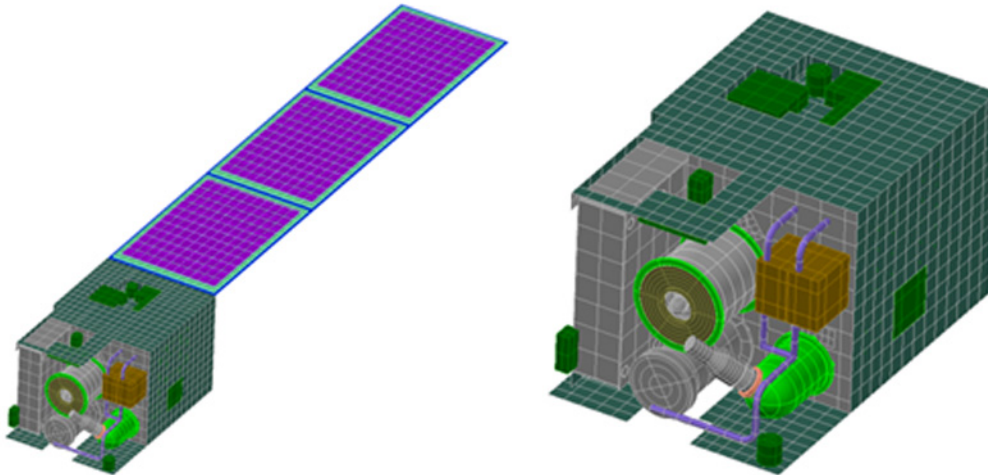

Figure 6. Image of the iSAT System Thermal Model with Solar Panels (left) and without Solar Panels (right).

B. Thermal Control

Thermal control components, including heaters and insulation, are required to maintain the feed system temperatures needed for sufficient propellant flow to the thruster and cathode. The tank and every feed line zone all have their own independently controlled external heaters and insulation. The tank heater is wrapped around the entire outer surface of the cylindrical shell, as well as on top of the tank lid. The valves are fabricated with independently controlled internal heaters and are also wrapped in insulation. Each of these heater zones uses on-off control with the heater duty cycle adjusted to achieve and maintain the temperature set points. The control sensor is located at the predicted coldest location in each heater zone. All insulation indicated has an effective emissivity of 0.01 and includes an outer layer of double aluminized Mylar. The double aluminum Mylar has optical properties of infrared emissivity=0.03 and solar absorptivity=0.12. The heater power and insulation type for each independent heater zone is given in Table 2. The cathode also has an internal heater necessary for operation, but it is not a focus of this study and will not be discussed further in this paper.

---

[a]A mass of 0.7 kg was used in the thermal modeling as it represented the original requirement for the iSAT mission (as opposed to the current iSAT propellant load requirement of 370 g).

Table 2. Propulsion Components Heater and Insulation Information.

Component	Heater Power [W]	On Temp [°C]	Off Temp [°C]	Sensor Location	Insulation Type	Outer Layer of Insulation
Feed Line Zone 1	2	115	125	Min Temp Location	MLI e^*=0.01	Double Al Mylar
Feed Line Zone 2	2	115	125	Min Temp Location	MLI e^*=0.01	Double Al Mylar
Feed Line Zone 3	2	115	125	Min Temp Location	MLI e^*=0.01	Double Al Mylar
Tank Zone	8	95	105	Min Temp Location	MLI e^*=0.01	Double Al Mylar
PFCV 1 (anode)	3	115	125	Internal	MLI e^*=0.01	Double Al Mylar
PFCV 2 (cathode)	3	115	125	Internal	MLI e^*=0.01	Double Al Mylar

C. Orbital Environments

Two orbital environments were modeled, one with a beta angle of 90° and one with beta angle of 0°. The environment with the beta angle of 90° will be referred to as the "hot environment" and the one with the beta angle of 0° will be referred to as the "cold environment." Additional details of these environments are listed in Table 3.

Table 3. Information for Thermal Modeling of Orbital Environments.

Parameter	Hot Environment	Cold Environment
Beta Angle [°]	90	0
Eclipse Time [min]	0	36
Sun Time [min]	96	60
Solar Flux [W/m^2]	1414	1322
IR Flux [W/m^2]	240	218

D. Thermal Modeling Results

Every normal phase of propulsion system operation was modeled. In Safe Mode, the thruster and feed system are not operating but other spacecraft components are still in operation (i.e. avionics, communications, power, etc.). For this mode, the components only need to stay above their respective survival temperature limits. For a typical 'Day-in-the-Life' mode of operation, there are three distinct operational periods for the propulsion system, and during each period the propulsion system thermal control components operate in a different manner. Specifically:

1. **Pre-Thrust Period**: Prior to thruster operation, the propellant tank, the feed line heaters, and the valve heaters turn on and heat the components to the required temperatures as indicated in Table 2.

2. **Thrusting Period**: During thruster operation, the heaters apply the power required to maintain the set-point temperatures in the different zones.

3. **Post-Thrust Period**: After thruster operation, the tank and feed line zones 2 and 3 heaters turn off immediately after thrusting. Feed line zone 1 heater and the valve heaters remain on to ensure that all iodine is deposited back in the cooling tank, rather than in the fuel lines and valves. After the tank has cooled to a specified temperature, these zones then also turn off.

While all the modes modeled are insightful in terms of guiding the design and operation of the spacecraft propulsion and power systems, for the sake of brevity we restrict our discussion in this paper to the pre-thrust period as it is the most demanding and power intensive for the propellant feed system heaters.

During the pre-thrust period, the PPU is switched on first. After this, the tank heater is activated since the tank and iodine propellant, possessing significantly more thermal mass than the rest of the feed system, take longer to heat. In this particular model, the tank heater is activated 94 minutes prior to thruster operation and all the feed line heater zones and valve heaters are activated 64 minutes prior to thrust. Not all heater zones operate at a 100% duty cycle. Instead, each heater cycles automatically based on the data received from its respective temperature sensor. Table 4 shows for each orbital scenario the time needed for each heater zone to reach the minimum required temperature, along with that zone's heater duty cycle and total operating time.

Table 4. Pre-Thrust Period Heater Operation Predictions.

	beta=0°			beta=90°		
	Time to Reach Temp [min]	Duty Cycle	Total On-Time [min]	Time to Reach Temp [min]	Duty Cycle	Total On-Time [min]
Feed Line Zone 1	50	0.88	56	42	0.78	50
Feed Line Zone 2	25	0.58	37	23	0.50	32
Feed Line Zone 3	20	0.55	35	19	0.48	31
Tank Zone	94	1.00	94	94	1.00	94
Valves	64	1.00	64	56	0.88	56

Figure 7. Temperature (in degrees Celsius) of propulsion components at a representative time during the pre-thrust period with beta=0°.
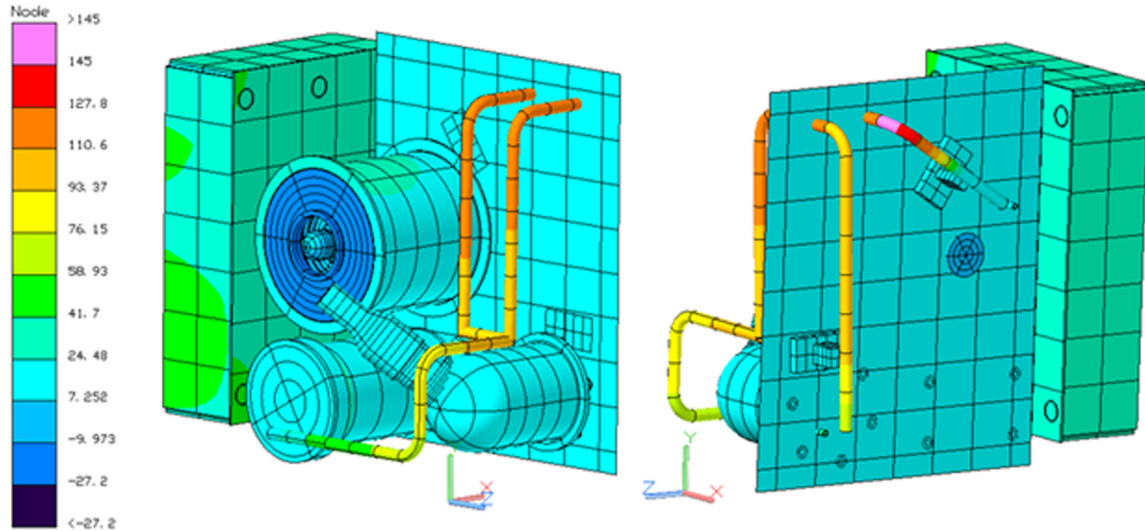

Figure 8. Temperature (in degrees Celsius) of propulsion components at a representative time during the pre-thrust period with beta=90°.

Contour plots of the pre-thrust period predicted temperatures (in degrees Celsius) for the beta=0° and beta=90° environments are shown in Figs. 7 and 8, respectively. Note that these plots do not correspond

to the final thermal end-state achieved during the pre-thrust period. They are instead representative time-points that show maximum thermal gradients in the propellant feed lines. Based on the specified heater power levels and locations and accounting for the overall spacecraft thermal environment, the propellant feed system components can be heated to their required temperature levels prior to operating the thruster.

VI.   Clog-Clearing Tests

In the iSAT propellant feed system, solid iodine is sublimed through heating to produce gaseous propellant that is conducted through tubing to the thruster and cathode. The sublimation process is governed by the iodine vapor pressure, which is shown as a function of temperature in Fig. 9. As iodine vapor flows out of the tank, the gas pressure in the volume around the solid iodine propellant is reduced until a balance between the flow of iodine out of the tank and the sublimation rate of solid iodine at the equilibrium gas pressure and chosen tank temperature is reached.
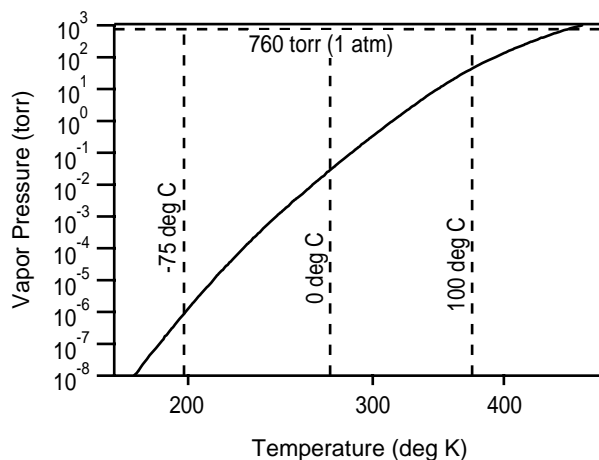

Figure 9. Vapor pressure curve for molecular iodine (I_2). After Refs. [8, 9].

One of the possible issues that can arise in an iodine propellant feed system is that the vapor can deposit to form a blockage/clog if a cold spot develops in the propellant lines, as occurred in the first integrated propulsion system test. In general, to keep iodine from redepositing in the propellant lines they should be kept significantly warmer than the solid iodine. In the flight system, the heaters will be designed to ensure that during normal operation the lines are always at a greater temperature than the tank. However, if a heater fails the line could still become clogged with iodine propellant.

The line heaters in iSAT have a secondary heater trace that can be used as a backup in the event that a primary heater fails. Such a failure would be detected by the iSAT PPU as either an open circuit (no current) or a short circuit (lower circuit resistance/higher current). In the present demonstration test, we aimed to purposefully create and clear an iodine clog in a tube, quantifying the timescale and relative difficulty of clearing. This testing was performed to show that in the event of a primary circuit heater failure the system could recover using the secondary heater circuit.

A.   Test Setup

The testing was performed in a 3-ft diameter, 6-ft long vacuum vessel. The chamber can be evacuated to high vacuum levels of 10^{-5}-10^{-6} torr using either a turbomolecular pump or, when iodine is flowing, a diffusion pump backed by a mechanical roughing pump. In addition, a Polycold refrigeration unit pumps chilled refrigerant (at -150°C) through an in-vacuum cooling coil. The coil serves to condense the iodine vapor providing a significant increase in the iodine pumping speed during a test. The vacuum chamber pressure is measured using an MKS Instruments 390 Micro-Ion ATM gauge with a recordable analog voltage output.

The flow system is shown schematically in Fig. 10. In the system, iodine loaded in the tank flows along the main line into vacuum. At the end of the line, the iodine exits into vacuum through a 0.028" OD orifice.
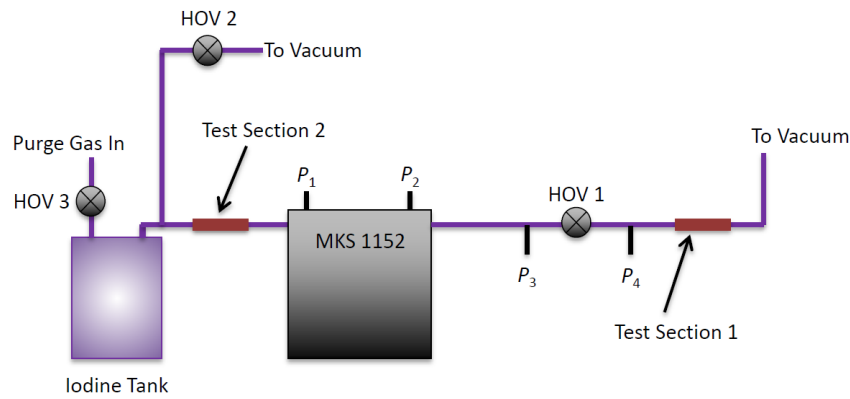
Figure 10. Iodine clog-clearing test flow system schematic.

The pressure is measured at 4 different locations within the system (P_1, P_2, P_3, P_4). The measurements P_1 and P_2 are within the MKS 1152 vapor phase flow meter, measuring the pressure at the ends of a laminar flow element to monitor the flow rate.

The pressures P_3 and P_4 are monitored by two Honeywell 2-psia hastelloy-bodied pressure transducers. Flow is controlled using hand-operated valves (HOVs) and solenoid-operated valves (SOVs), with HOV2 making it straightforward to evacuate the tubing upstream of the vapor-phase flow meter.

At the test section locations, a piece of bent glass tubing is inserted into the line in the manner depicted in Fig. 11. The flowpath is broken and the routing directed downward where it is mated to a glass tubing section using a Cajon O-ring sealed fitting. The glass section has two bends directing the iodine flow back upward to continue flowing towards the vacuum chamber. During the test, the glass section is first heated to the same temperature as the rest of the line and then immersed in an ice water bath, cooling the walls to produce an iodine clog at that location. The use of glass tubing permits the visual verification that clogging is occurring.
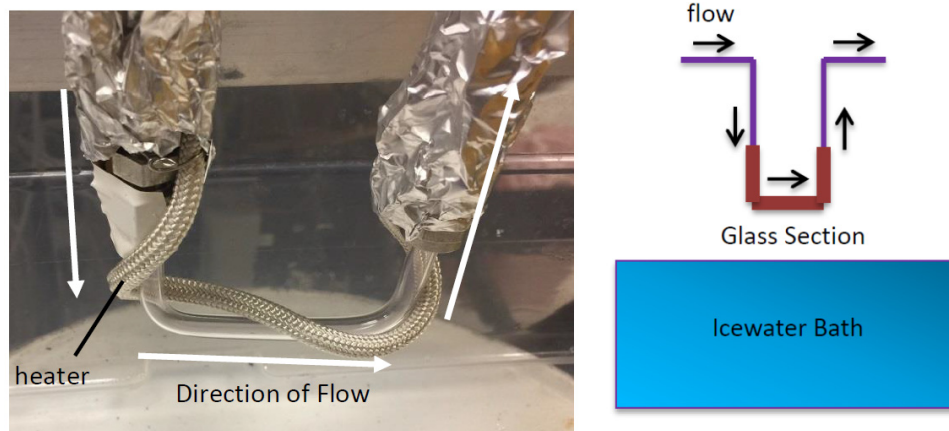

Figure 11. (left) Glass tube inserted into the flowpath. (right) Schematic of the glass tube test section.

B.   Test Results

The illustration in Fig. 10 showed two possible locations where an iodine clog could be produced in the present setup. When there is an iodine flow, the largest pressure drop in the system occurs across the MKS 1152 vapor flow meter. Consequently, the two test sections correspond to a lower-pressure location (test section 1) and a higher-pressure location (test section 2). We report below on testing conducted in each section.

1. Test Section 1

The iodine pressure in test section 1 is always low (well below 10 torr throughout the test). During testing an iodine flow was initiated by opening valve HOV1. After the flow was established, the glass tubing was exposed (overwrapped aluminum foil and heater rope removed from that section) and submerged into an ice bath producing the start of a clog in a matter of seconds.
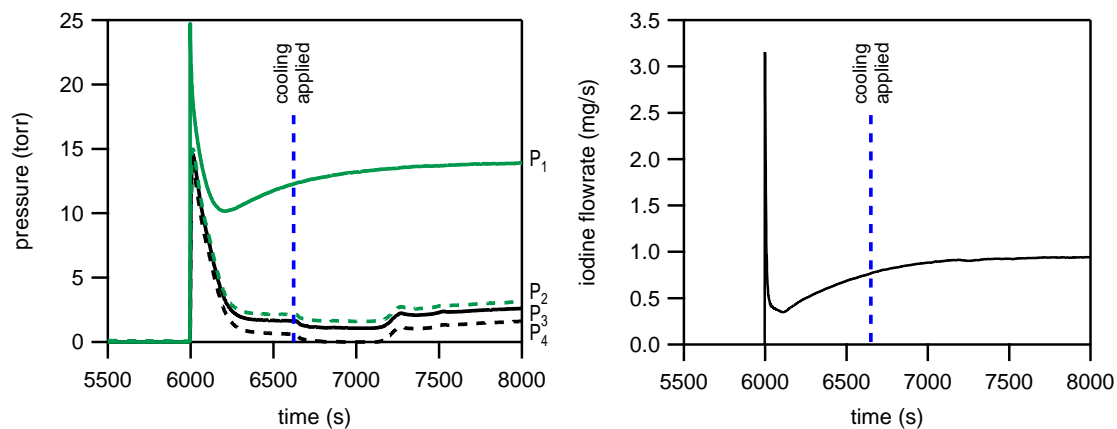

Figure 12. For the experiment in test section 1, while the clog was formed: (left) gas pressures measured along the flowpath and (right) iodine flowrate measured by the MKS 1152 flow meter.
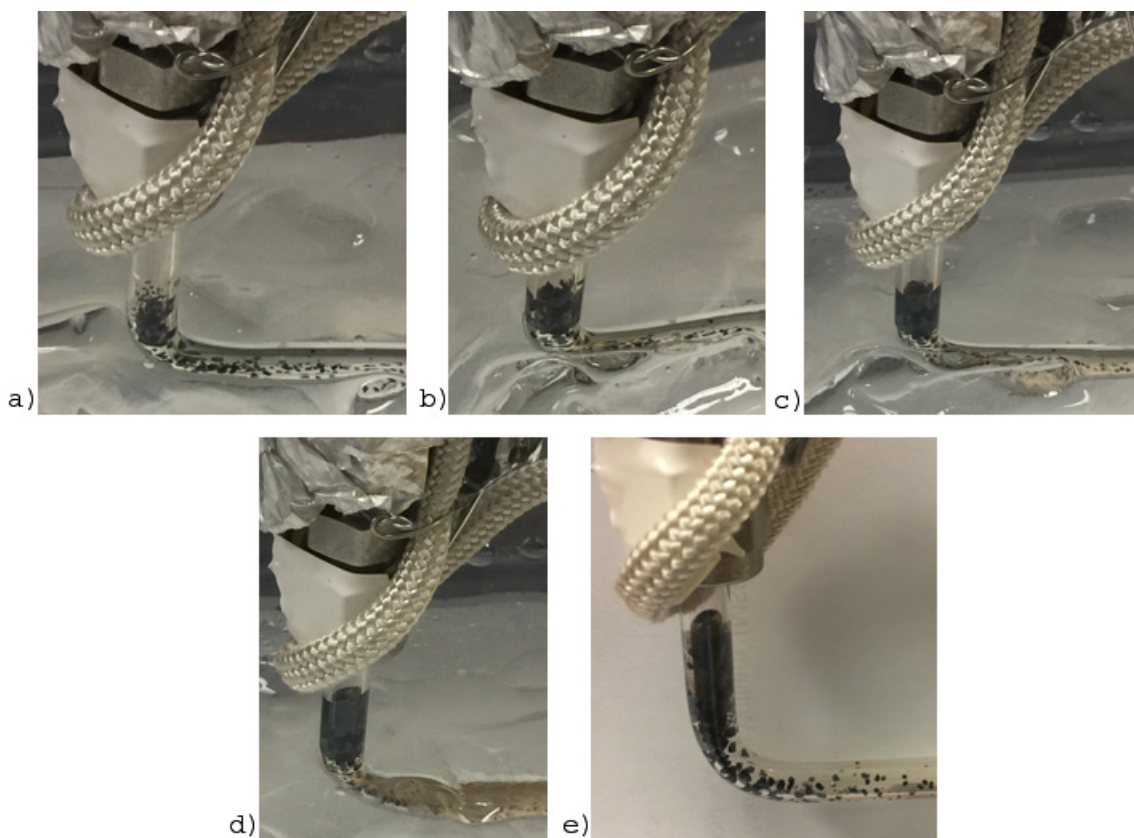

Figure 13. For the experiment in test section 1, sequence of images of the iodine plug as it was forming, where a) was immediately after immersion in the ice water bath and e) was immediately after removal from the ice water bath approximately **2.75 hours** after initial immersion.

The measured iodine pressures and iodine flowrate are presented in Fig. 12 for the beginning of the test, with the time when the glass tubing was submerged in the ice bath denoted as 'cooling applied'. The reduction of the gas pressure as measured by gauges P_2, P_3, and P_4 was immediate, as was the appearance of iodine deposition on the glass tubing walls, preferentially appearing where the glass first enters into the cold water. The clog evolution as a function of time is shown in Fig. 13, with 13a being an image just after the tubing was submerged in the ice bath and image 13e at a time 2.75 hours later just before heating is reapplied to clear the clog.

The pressures and iodine flowrate for the period of time when heating was reapplied to the test section and the clog was cleared are presented in Fig. 14. At an experiment time of approximately 16650 s the pressure trend reverses, indicative of clog clearing. Within 5 minutes of applying heat the clog was completely gone from this section. We note that at no time during this testing was the measured flow reduced to zero; in fact it mostly remained constant at between 0.8 and 1.0 mg/s.
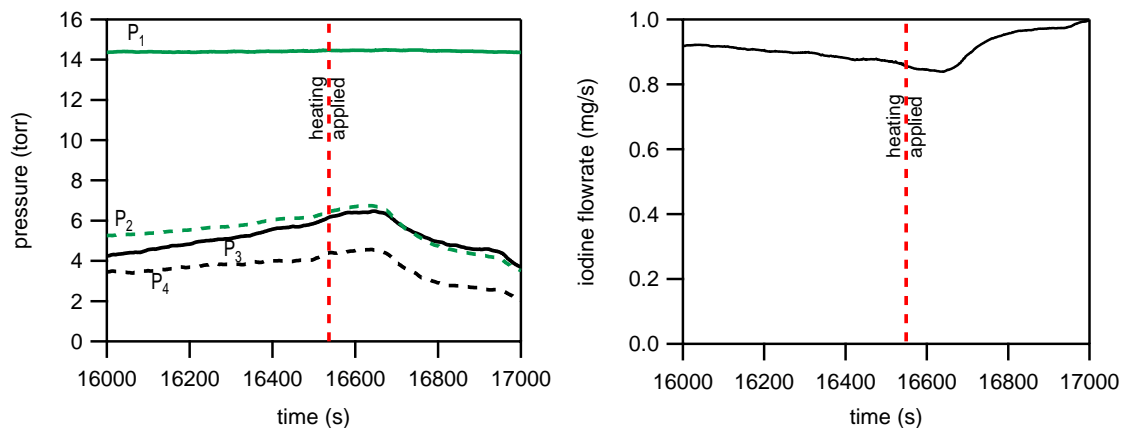

Figure 14. For the experiment in test section 1, while the clog was being cleared: (left) gas pressures measured along the flowpath and (right) iodine flowrate measured by the MKS 1152 flow meter.

2. Test Section 2

When the flowpath is clear the pressure in test section 2, minus any small line losses, is roughly equal to the pressure in the tank. The time histories of the pressure and iodine flowrate for this trial are presented in Fig. 15. The iodine tank was heated to temperature and then the test section was immersed in the ice water bath with HOV1 closed. With the tank at elevated temperature but no iodine flow yet established, only a faint ring of iodine can be observed depositing on the glass tube where it enters the water (Fig. 16a). This ring is formed from iodine that moved from the iodine tank into the tube purely through diffusion. Once HOV1 was opened permitting iodine to flow, the formation of a clog, shown in Figs. 16b and 16c, was very rapid. The flowrate was almost immediately reduced to a no flow condition when this clog formed. Comparing Fig. 13e and Fig. 16c, we observe that the plug appearing in the test section is much longer and appears to more completely fill the tubing in the latter image.

The clog clearing process was accomplished with HOV1 open throughout the duration of the test. Relative to the clog in test section 1, the clog in this case took much longer to disappear and the limited thermal conductivity of glass made it difficult to heat the glass tubing from an initially-cold condition. Iodine underneath the path of the rope heater was observed to disappear first, with iodine further away remaining longer. Mid-way through the test a heat gun was added to supplement the rope heater on test section 2 ('added clog heating' in Fig. 15) so the test could be completed in a reasonable amount of time. The iodine in the clog actually served as an iodine sublimation source and as it was elevated in temperature to the level of the rest of the flowpath, the flow rate increased dramatically between the experiment time of 5000-6000 s. The flow rate out generally decreased after the tank heater was turned off to limit the supply of iodine to that subliming from the clog. Many of the ups and downs in the pressure and flow rate were due to outside events, such as the moving of a rope heater to give it better thermal contact, the addition of the heat gun to increase the temperature of the entire test section more quickly, or the removal of insulating foil to visually
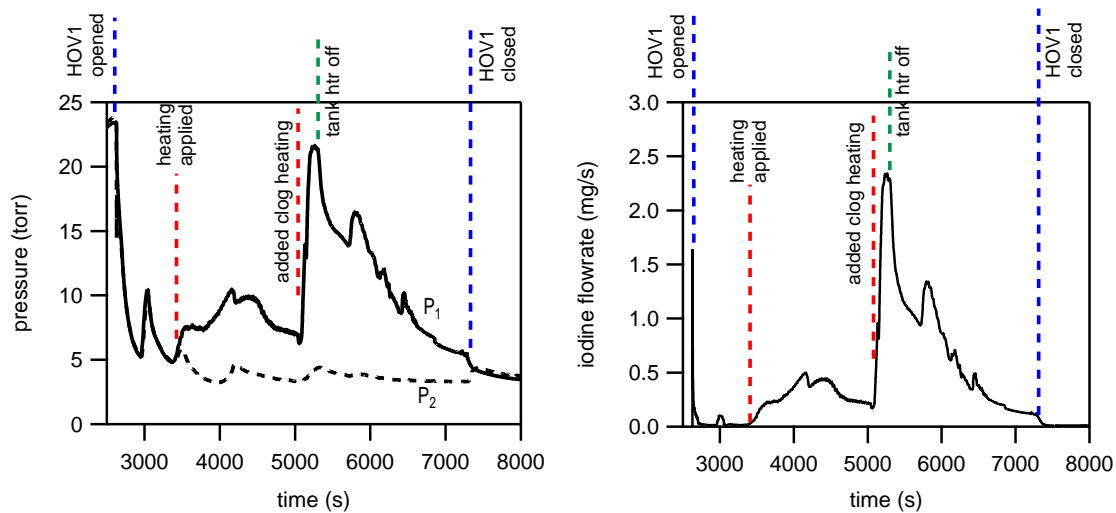
Figure 15. For the experiment in test section 2, time histories showing: (left) gas pressures and (right) iodine flowrate measured by the MKS 1152 flow meter. Data span the clogging and clog-clearing process, with the time of discrete events indicated.
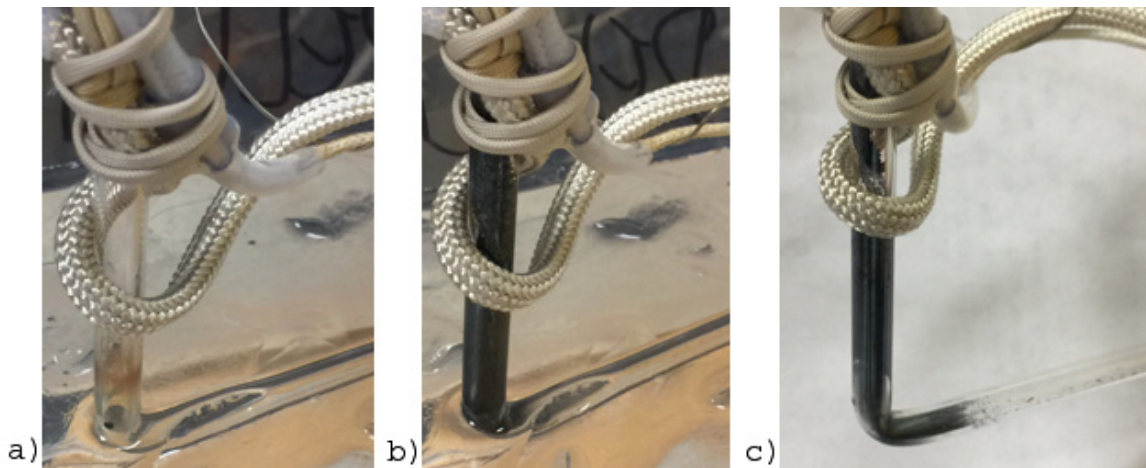

Figure 16. For the experiment in test section 2, sequence of images of the iodine plug as it was forming, where a) was immediately after immersion in the ice water bath, b) was just after the opening of HOV1, and c) was immediately after removal from the ice water bath approximately 15 mins after initial immersion.

observe the clog-clearing progress.

C. Discussion of Results

The formation of solid iodine in test section 1 and the initial drop in the pressures measured by gauges P_2, P_3, and P_4 indicated that as the deposit first formed the cold section was actually removing iodine from the gas phase faster than it was entering the test section. Effectively, the tank was producing iodine vapor while the cold section was removing it from the gas phase, permitting flow to continue across the flow meter. Later in the testing the pressures increase to a level greater than when the tube is unclogged, but they do not approach the value of P_1, which remains relatively constant throughout the test. We conclude that the clog, while capturing some of the iodine in that region, is also somewhat porous allowing some iodine to pass. A comparison of the photographs in Figs. 13 and 16 show that the extent and apparent density of the deposit in test section 1 was much smaller than the clog that formed in test section 2. The clog in test section 1 cleared within a few minutes of the removal from the water bath and the reapplication of heating. The test section 1 data where a clog was formed in the low pressure section of a feed system (the section

directly exposed to vacuum conditions) allow us to conclude that a clog in this area will be small in extent, will not completely block the flow, and will be relatively easy to clear.

By contrast, visual observations of the clog formed in test section 2 showed it to be much larger in extent and apparent density, forming to that size very quickly (10s of seconds), as compared to the hours it took to form the small plug-like clog in test section 1. The clog could be cleared, but it took significantly longer to do so relative to test section 1. The problem was exacerbated by the poor heat transfer properties of glass, which did not reheat quickly after the tubing was removed from the water bath. Note that the test section heaters were part of the heater zone consisting of all the tubing outside of the vacuum tank. This heater zone was regulated based upon a temperature measurement at a different location (SOV1), which was always hot, so the average heater power applied during the unclogging phase was actually less than the average power applied during initial heating of the system. This lower level of average power was not effective in reheating the glass tubing section in a timely manner, necessitating the use of the heat gun to supplement the overall heating.

In the flight system, while the heaters are designed to ensure that the lines remain hotter than the propellant tank, a heater failure could cause a propellant line to become clogged with iodine propellant. The iSAT flight system possesses a set of redundant heaters to permit clearing the blockage through the application of heat if a primary heater circuit fails. The testing showed that the manner in which the clog forms and is cleared is highly dependent upon the location in which the clog forms.

- The low-pressure section near the exit to vacuum is relatively difficult to completely clog, with clog-clearing through the application of heat being very easy and quick.

- The high-pressure section near the sublimation source is very easy to clog completely, but much more difficult to clear as it requires significantly more time and heat.

VII. Flow Modeling

A. GFSSP

Numerical models of the propellant feed system and associated laboratory test configurations were implemented using the Generalized Fluid System Simulation Program (GFSSP), version 7. GFSSP is a general-purpose lumped-element CFD program used for modeling complex flow networks.[10] Both steady-state and unsteady fluid behavior may be modeled. In addition, one can include conjugate heat-transfer and fluid and phase mixtures. GFSSP includes extensive existing component libraries (pipes, tees, elbows, flow restrictions, etc.) with models for their flow resistance. It also contains the thermo-physical properties for a variety of fluids. It includes thermal properties for a variety of solid materials, necessary when the conjugate heat transfer option is used. The code has been validated against numerous text book problems with closed form solutions and, whenever possible, against actual test data.

B. Iodine Properties

There is not a great deal of data on the thermo-physical properties of iodine, and what information is available is often given only over a limited range of conditions. For some properties, data were available over the full temperature range of interest; for other properties, values had to be extrapolated. Much of the data that was found was for iodine vapor at a pressure of about one atmosphere; much higher than the operating pressure of the propellant feed system. Data for gaseous F_2, Cl_2, and Br_2 were sought, as they might serve as guides to the behavior of iodine. However, information on these other halogens was even scarcer. Where there were gaps in the iodine data, nitrogen was used as a guide to its behavior as it is also a diatomic molecule

The seven fluid properties were calculated over a 51×72 matrix; 51 points uniformly spanning the pressure range from 7×10^{-5} Pa (10^{-8} psi) to 34.47 kPa (5.0 psi) and 72 points spanning the temperature range 10^{-8}, 100, 105, ..., 450 K. The initial point in the temperature array at essentially zero temperature (T = 10^{-8} K) was added to prevent GFSSP from going out of range during the solution iterations. The properties were converted from MKS to imperial units and written to the fluid property files for use with GFSSP. What follows is a brief description of how these fluid properties were obtained and regularized for use with GFSSP.

1. Specific Heat (C_p), Enthalpy (H), and Entropy (S)

These properties are taken from the NIST-JANAF tables,[11] which are based on a variety of sources, including experiments and ab-initio calculations. For each of these quantities, eight discrete values over the range of 100 K to 450 K were obtained from the reference and then interpolated to a 71 point array using a cubic-spline interpolation. This method yields an interval of 5 K per point, which is sufficiently fine to reflect the behavior of these properties as a function of temperature. The NIST-JANAF data are given for a pressure of 1 bar, however application of the thermodynamic relations can be used to deduce the pressure dependence of these quantities. To 0th order, C_p and H are independent of pressure. The pressure dependence of the entropy S is found by considering the first law of thermodynamics, $T\,dS = dU + P\,dV$, and using the ideal-gas relation to yield

$$S(P,T) = S_0(T) - R\ln\left(\frac{P}{P_0}\right) \tag{1}$$

where R is the universal gas constant, and S_0 is the entropy (at the given temperature) at the reference pressure $P_0 = 1$ bar. Data for N_2, located in the NIST database,[12] were examined for the same temperature and pressure range under consideration here and it was found for nitrogen that C_p and H were indeed approximately constant as a function of pressure and that S varied with pressure according to Eq. (1), giving confidence for the method employed herein.

2. Ratio of Specific Heats (γ)

The specific heat ratio was calculated from the formula $\gamma = C_p/C_v = C_p/(C_p - R)$.

3. Thermal Conductivity (κ)

Data for the thermal conductivity of I_2, plotted in Fig. 17a, was found over the range of 400 - 600 K [13]. The pressure range cited for these data was 26.7 - 59.3 kPa, although it was not stated what pressure applies for any given value of $\kappa(T)$.
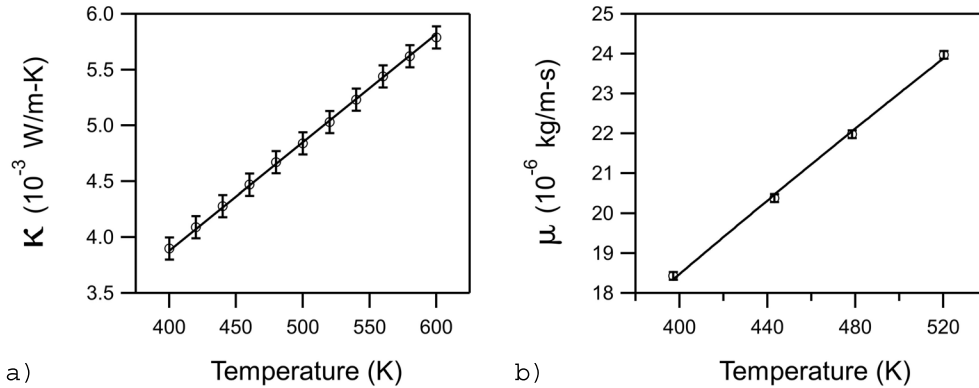

Figure 17. a) Thermal Conductivity of I_2 as a function of temperature, taken from Ref. [13]. Also shown is a linear fit to the data, $\kappa = a\,T$, with $a = (9.70 \pm 0.06) \times 10^{-6}$ W/m-K^2. b) Measured viscosity of I_2 as a function of temperature, taken from Ref. [14]. Also shown is a fit to the data using Sutherland's formula (Eq. (2)) with $\mu_0 = (3.85 \pm 0.36) \times 10^{-5}$ kg/m-s and $T_0 = (417 \pm 41)$ K.

Comparing the iodine data with available data for nitrogen, we found that the thermal conductivity of N_2 varies linearly with temperature and does not vary appreciably with pressure over the entire temperature and pressure ranges of interest. By analogy, we assume that the thermal conductivity of I_2 is relatively independent of pressure and that the values can be linearly extrapolated down to lower temperatures. A linear fit to these data was performed, of the form $\kappa = a\,T$, resulting in a slope $a = (9.70 \pm 0.06) \times 10^{-6}$ W/m-K^2.

4. Viscosity (μ)

Measurements of the viscosity of I_2, plotted in Fig. 17b, have been reported over a temperature range of roughly 400 K - 520 K [14]. These measurements were performed at a pressure of 6.0 kPa (the vapor pressure of sublimed iodine at a temperature of 373.15 K). This pressure is within the expected operating range of the iSAT propellant feed system. As for previous properties, nitrogen was used as a guide to determining the behavior of iodine as a function of temperature and pressure. The viscosity of N_2 increases monotonically with temperature and is independent of pressure. Over the temperature range considered, μ appears to vary linearly with temperature, however the dependence of viscosity with temperature (for temperatures > 100 K) is generally thought to be better described by Sutherland's formula[15]

$$\mu(T) = \mu_0 \frac{(T/T_0)^{3/2}}{(1 + (T/T_0))} \tag{2}$$

The data shown in Fig. 17b were fit with Eq. (2), with μ_0 and T_0 treated as fitting parameters, yielding $\mu_0 = (3.85 \pm 0.36) \times 10^{-5}$ kg/m-s and $T_0 = (417 \pm 41)$ K. A linear fit yielded a lower reduced fitting parameter, however it diverged significantly from the fit to Eq. (2) at lower temperatures. Given that Sutherland's formula is the generally accepted form for the temperature dependence of viscosity, it was used to generate the I_2 property tables over the range of interest.

5. Density (ρ)

The density is calculated using the ideal gas law, $P = nkT$, such that

$$\rho(P,T) = m_{I_2} n = \frac{M_{I_2} m_{\text{amu}}}{k} \frac{P}{T} \tag{3}$$

where k is Boltzmann's constant, M_{I_2} is the molecular mass of I_2 (253.809 amu), and m_{amu} is the mass of one amu (1.66054×10^{-27} kg).

C. Sublimation Model

The sublimation of solid iodine into vapor was included in the GFSSP model. The quasi-steady rate of mass evolution for the sublimation of a solid can be calculated as[16, 17]

$$\frac{dm}{dt} = \alpha A \sqrt{\frac{M}{2\pi RT}} (P_{vap} - P) \tag{4}$$

where α is a sticking coefficient (usually assumed to be 1), A is the exposed surface area, M is the molar mass of the solid material, R is the universal gas constant, P and T are, respectively, the ambient pressure and temperature of the overlying gas, and P_{vap} is the vapor pressure at the temperature of the solid being sublimed. This equation assumes that the solid and the overlying gas are in approximate equilibrium.

The sublimation of mass into the tank was implemented in the model by including a mass source term in GFSSP that is governed by Eq. (4). The rate of mass evolution in the tank node is calculated at every time-step using the updated fluid and solid node variables. A back-relaxation scheme was used to make the calculation numerically stable.

D. Component Models

A wide variety of components can be modeled in GFSPP and are available as standard options. Valves, for example, can be modeled with either the flow-restriction or compressible orifice option by providing a history file with a time-dependent orifice area. This approach assumes that the flow coefficient, C_f, providing the relationship between the pressure drop across the component and the corresponding flow rate, is well known. This is the case for standard flow system elements, such as straight sections of tubing, elbows, and tees, and for commercially available valves, characterized for and used within their nominal operating regime.

The iSAT PFS makes use of two custom build PFCVs. These valves regulate the flow of propellant to the anode and cathode. The valves have not been characterized for the low flow rates that will be seen in the iSAT PFS. Likewise, the anode of the HET is a custom-built component, and its behavior is not known *a priori*. In the low Reynolds number regime of the PFS, the behavior of the valves will be dominated by

the viscous flow in the boundary layer, and this will be highly dependent on the specific geometry of the component. Consequently, the value of C_f for each component should be measured under likely operating conditions, as models for these components are needed for the overall GFSSP model.

Tests on a valve (different than the PFCVs used in the iSAT system) were conducted to develop the process by which the value of C_f could be measured. Tests were performed with N_2 as the working fluid under the assumption, discussed previously, that N_2 is a suitable flow simulant for I_2. The results of these tests are shown in Fig. 18. The valve was installed in a simple test line consisting of 6.35 mm (1/4") o.d. stainless-steel tubing; the same size tubing to be used in the actual iSAT PFS. Nitrogen was supplied from a K-bottle and the test line was exhausted into a vacuum chamber. The volumetric flow-rate through the valve was set using an MKS 1479A flow controller located upstream of the valve, while the pressure and temperature in the line were measured immediately upstream and downstream of the valve. The data indicate the problem of parameterizing the operation of the valve in terms of the pressure. In Fig. 18a, although the curves all seem to approach a common limiting curve at higher values of P_{up}, they diverge significantly at lower pressures. In terms of $P_{\mathrm{up}}/P_{\mathrm{down}}$ shown in Fig. 18b, the three curves are widely dispersed and no simple parameterization of the flow is apparent.
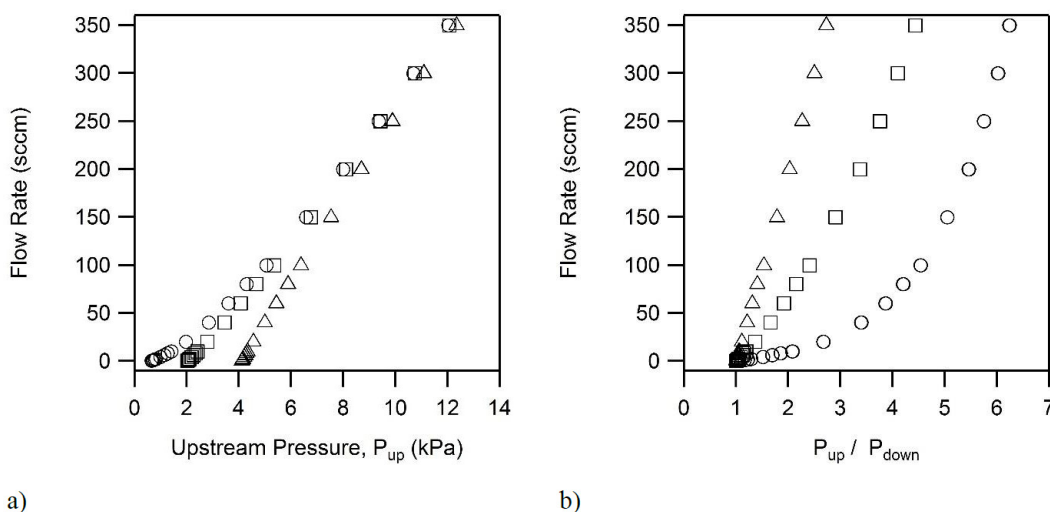

Figure 18. N_2 flow-rate through the valve versus a) upstream pressure, and b) the ratio of upstream to downstream pressure, for three values of the background pressure in the exhaust chamber: ○ ~667 Pa (5 torr), □ ~2,000 Pa (15 torr), △ ~4,000 Pa (30 torr).

Parameterization of the flow through the device in terms of Reynolds number was suggested[18] as being a method that could readily be integrated into a GFSSP model. The flow coefficient and Reynolds number for these data were deduced using a simple generic steady-state GFSSP model that can be used for a variety of components. The device-under-test is modeled using the compressible orifice component in GFSSP. The pressures and temperatures measured in the experiment at both the upstream and downstream test stations are specified as the boundary conditions in the external nodes of the GFSSP model. The measured volumetric flow rate was converted to a mass flow rate using tables of densities for N_2 over the relevant pressure and temperature range, and a bi-linear interpolation scheme was used to determine the density for the specific measured values of upstream pressure and temperature. The compressible orifice area was fixed (1.94×10^{-6} m^2) and the value of C_f was varied until the flow rate predicted by GFSSP equaled the measured value (the agreement in flow rate was typically good to three or four significant figures). This value of C_f was recorded with the Reynolds number calculated by GFSSP. The resulting curves of $C_f(Re)$ are shown in Fig. 19. The results from all three tests in Fig. 18 collapse to one curve of the form

$$C_f = \alpha \, Re^n \tag{5}$$

where α and n are the fit parameters. The data collapse with relatively little dispersion indicating the utility of the proposed parameterizing of C_f in terms of Reynolds number.
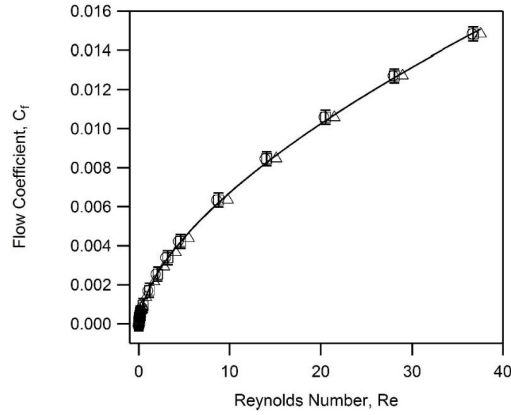
Figure 19. Flow coefficient as a function of Reynolds number for the data in Fig. 18, as deduced with GFSSP. Data for three separate trials with different back-pressures: ○ ∼**667 Pa (5 torr),** □ ∼**2,000 Pa (15 torr),** △ ∼**4,000 Pa (30 torr).**

E. Flow Modeling Results

While several cases and configurations were modeled, we focus on only a couple here for the sake of brevity. Specifically, we discuss models based upon the geometry of the clog-clearing tests presented in Fig. 10.

A blow-down test was conducted by charging the tank with N_2 and then opening HOV1 to evacuate it to vacuum. Much of the testing and model validation was performed using N_2. Nitrogen, like iodine vapor, is diatomic; it is therefore assumed that the two species behave similarly in many respects and that nitrogen can be used as a relatively good simulant for iodine. It is also easier to work with N_2 in the lab environment and there exists a wealth of data regarding its fluid properties over wide ranges in pressure and temperature. The results of the experiment along with that of the corresponding GFSSP calculations are shown in Fig. 20. For the calculation, the terminal orifice was assumed to have a flow coefficient of C_f=0.05. A variable flow coefficient was specified for the valve; $C_f = 0.0005 \cdot Re^{0.6}$ was found to yield the best overall agreement with the data.
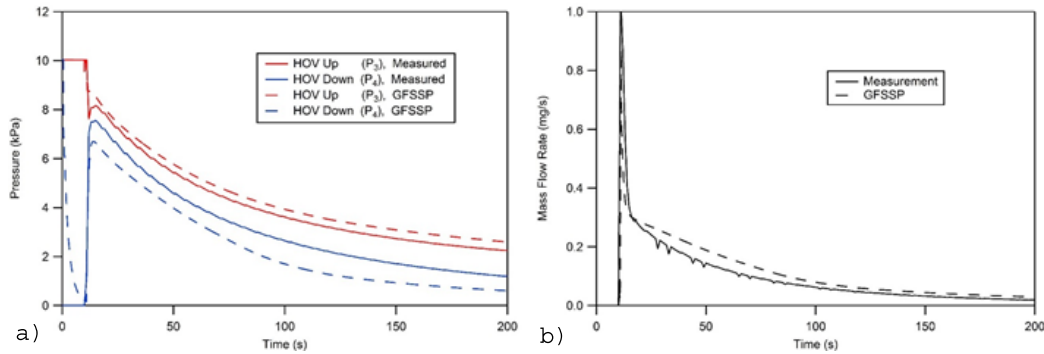

Figure 20. Results of a blow-down test with N_2: a) experimentally measured and GFSSP-calculated pressures upstream and downstream of the HOV1. b) Measured and calculated mass flow rates.

The GFSSP calculations show qualitative agreement with the data, and at least order of magnitude quantitative agreement. Attempts to coax better agreement from the calculation by varying the orifice flow coefficient or the effective hydraulic diameter of the flow meter's laminar flow element were unsuccessful and sometimes caused the solutions to become unstable.

Clogging tests of Sect. VI provided an opportunity to compare the sublimation model with test data. For the test section 1 experiment, a glass section was added downstream of the HOV1, so that clogging of the line due to iodine redeposition could be observed. After the tank had warmed to a temperature of 87°C, the valve was opened and the iodine allowed to flow. In the test, the feed-line was held at a higher temperature
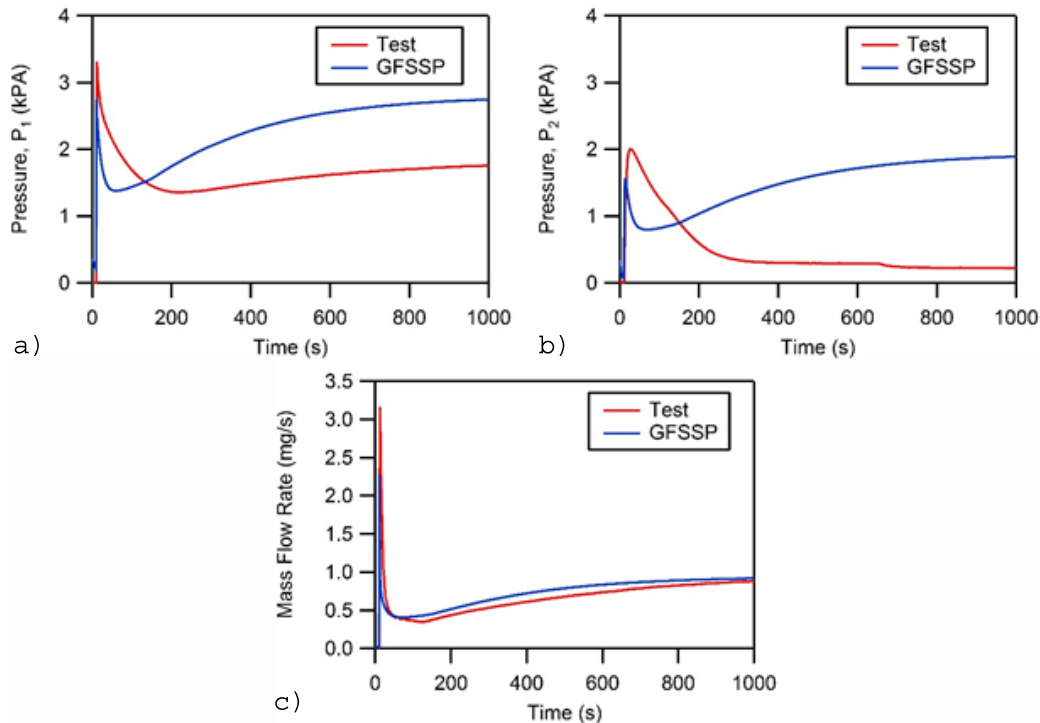
Figure 21. Comparison of test data (from the setup in Fig. 10) and the GFSSP model with iodine: a) pressure at station P_1, b) pressure at station P_2, and c) the mass flow rate.

than the iodine tank, however any heat transfer from this line into the iodine is not modeled in GFSSP. Clogging was observed, however iodine continued to flow and deposit at the clog site. In that sense, the downstream clog just acted as an iodine sink, having little effect on the source, which continued providing a flow of iodine as if the gas was being exhausted into the vacuum chamber.

The GFSSP model is essentially the same as that used for the blow-down testing, but with the addition of a solid node representing the solid iodine in the tank. This node is in thermal contact with the tank wall as well as with the vapor in the ullage region. Constant flow coefficients are used throughout the calculation. The results of this test, along with the corresponding GFSSP results, are shown in Fig. 21. The initial pressure in the ullage region was chosen to be 4.14 kPa, so as to more closely match the initial peak in pressure seen in the data; the vapor pressure of I_2 at the initial temperature is 1.52 kPa. The calculated pressures are qualitatively similar to the measured pressures, though the two have significant quantitative differences, especially the pressure downstream of the flow-controller. However, it should be noted that the conditions further downstream of station P_2 were less well known (due to the clog that was forming), so it is perhaps unsurprising that the GFSSP model (which assumed an unclogged line) had difficulty in reproducing the pressure. The calculated flow-rate agrees with the measured flow-rate, both qualitatively and quantitatively, reaching an asymptotic value (i.e. steady-state) of about 1 mg/s and indicating that the GFSSP model is able to simulate the transient sublimation process with a reasonable degree of fidelity.

F.   Discussion

With the GFSSP models employed, it has been possible to match qualitative trends observed in actual test data, but achieving quantitative agreement has been more difficult. Most of the feed system can be modeled with standard GFSSP components: pipes, tees, elbows, etc. However, the most critical components, such as the PFCVs, anode, and cathode, are limiting orifices and need to be treated as such. The compressible orifice option in GFSSP has been used for these components. It requires, as inputs, the orifice area and flow coefficient. For the PFCVs, the areas and flow coefficients are not necessarily known at all times.

Based upon the testing described above, we can expect flow coefficients for orifices to be low and highly dependent on the Reynolds number. Typical values for Reynolds number in the iSAT propellant feed system

are Re≤100. The mean free path, λ, of an I_2 molecule under the conditions typical for iSAT can be estimated as:

$$\lambda = \frac{1}{n\,\sigma} \tag{6}$$

where σ is the collision cross-section of the molecule and n is the number density, given as $n = \rho/m_{I_2}$ with ρ=0.064 kg/m^3, and the mass of an iodine molecule m_{I_2}=4.2×10^{-25} kg. The cross-section can be estimated as

$$\sigma = \pi\,r_{VdW}^2 \tag{7}$$

where r_{VdW} is the Van der Waal's radius, wich for I_2 is 0.198 nm. Using these numbers yields a mean free path λ=50 μm. The i.d. of the tubing used in the feed system is 4.57 mm, about 90 times greater than λ. Boundary layers are typically assumed to be a few hundred mean free paths thick, so one can conclude that the entire iSAT propellant feed system is, under most circumstances, in a highly viscous, boundary-layer-like regime. For the PFCVs, the linear distances could be even smaller, so that not only is the flow highly viscous, but the fluid assumption itself might begin to break down. For these reasons, it is perhaps not surprising that it was often difficult to obtain quantitative agreement between the model and test data. The typical flow regimes in iSAT are likely at or beyond the very low end of what GFSSP was developed to simulate.

VIII. Conclusion

An integrated test of the iSAT development thruster, cathode, and propellant feed system was conducted in 2016, and while the system operated for a short time and had several successes – most notably the operation of the cathode and thruster fed simultaneously from a single iodine propellant reservoir – the testing revealed design deficiencies and risks that required further development work to retire. In this paper we have presented a summary of the development work that was performed to further develop and improve upon the propellant feed system design. The original propellant control valves had significant materials-compatibility issues when exposed to iodine vapor, necessitating a redesign to use materials that are more resistant to iodine chemical attack. Dynamic modeling and analysis of the feed system exposed high-stress vibrational modes in the feed lines. These levels were reduced to within a positive margin of safety through the inclusion of additional tubing constraints on the backside of the propulsion plate. Thermal modeling of full spacecraft was conducted and showed that, for the assumed heater power budget and modeled orbital environments, the propellant feed system components could be heated to their required temperature levels prior to operating the thruster. The clogging of an iodine propellant line was experimentally investigated to determine if the feed system could recover from the formation of a clog through iodine deposition. It was found that iodine clogs occurring at low-pressure (near vacuum) conditions were difficult to form and relatively easy to clear, while those clogs occurring at high-pressure (near to the pressure of the propellant tank) were very easy to form and took considerable time to clear. An extensive effort was made to collect a set of iodine thermo-physical properties at the operating conditions of the feed system to support fluid flow and sublimation modeling. The flow modeling was able to match qualitative trends observed in actual feed system experimental data obtained for nitrogen and iodine flows, but it was difficult at the low flow levels associated with iSAT to obtain quantitative agreement. This was likely because of the highly viscous nature of the flow and the highly Reynolds number-dependent nature of component flow coefficients in this low-flow regime, which is likely near or below the limit where the GFSSP modeling program can be applied.

References

[1] *CubeSat Design Specifications*, rev. 13, The CubeSat Program, California Polytechnic State University, San Luis Obispo, CA (2014).

[2] J. Szabo, B. Pote, S. Paintal, M. Robin, A. Hillier, R.D. Branam, and R.E. Huffman, "Performance Evaluation of an Iodine-Vapor Hall Thruster," *J. Propuls. Power* Vol. 28, No. 4, pp. 848–857 (2012).

[3] J.W. Dankanich, K.A. Polzin, D. Calvert, and H. Kamhawi, "The iodine Satellite (iSAT) Hall Thruster Demonstration Mission Concept and Development," in *50th AIAA/ASME/SAE/ASEE Joint Propulsion Conference*, Cleveland, OH (2014). AIAA Paper 2014-3910.

[4] K.A. Polzin, S.R. Peeples, A.O. Burt, A.K. Martin, A. Martinez, J.F. Seixal, and S. Mauro, "Development, Demonstration, and Analysis of an Integrated Iodine Hall Thruster Feed System," in *AIAA Propulsion and Energy Forum 2016*, Salt Lake City, UT (2016). AIAA Paper 2016-4730.

[5] K.A. Polzin, S.R. Peeples, J.F. Seixal, and S.L. Mauro, B.L. Lewis, G.A. Jerman, D.H. Calvert, J. Dankanich, H. Kamhawi, T.A. Hickman, J. Szabo, B. Pote, and L. Lee, "Propulsion System Development for the Iodine Satellite (iSAT) Demonstration Mission," in *34*th *International Electric Propulsion Conference*, Hyogo-Kobe, Japan (2015). IEPC Paper 2015-09.

[6] *General Environmental Verification Standard (GEVS)*, Technical Standard GSFC-STD-7000A, NASA-Goddard Space Flight Center, Greenbelt, MD (2013)

[7] J.W. Miles, "On Structural Fatigue Under Random Loading," *J. Aeronautical Sci.*, Vol. 21, No. 11, pp. 753–762 (1954).

[8] R.E. Honig, "Vapor Pressure Data for the Solid and Liquid Elements," *RCA Rev.*, Vol. 23, pp. 567–586 (1962).

[9] R.E. Honig and D.A. Kramer, "Vapor Pressure Data for the Solid and Liquid Elements," *RCA Rev.*, Vol. 30, pp. 285–305 (1969).

[10] A.K. Majumdar, A.C. LeClair, R. Moore, P.A. Schallhorn, *Generalized Fluid System Simulation Program, Version 6.0*, NASA TP-2016-218218, NASA-Marshall Space Flight Center, Huntsville, AL (2016).

[11] NIST-JANAF Thermochemical Tables, *J. Phys. Chem. Ref. Data*, Monograph 9, pp. 1417 (1982).

[12] NIST Chemistry WebBook, *Thermophysical Properties of Fluid Systems*, National Institute for Standards and Technology, http://webbook.nist.gov/chemistry/fluid (2016).

[13] N.B. Vargaftik and L.P. Filippov, *Handbook of Thermal Conductivity of Liquids and Gases*, CRC Press, pg. 36 (1994).

[14] A.O. Rankine, "On the Viscosity of the Vapour of Iodine," *Proc. Royal Soc. London: Series A*, Vol. 91, No. 627, March 1, pp. 201-208 (1915).

[15] B.D. Tapley and T.R. Poston (eds), *Eshbach's Handbook of Engineering Fundamentals, 4th Edition*, John Wiley & Sons, Inc., pp. 6-11 (1990).

[16] I. Langmuir, "The Constitution and Fundamental Properties of Solids and Liquids: Part I. Solids," *J. Am. Chem. Soc.*, Vol. 38, pp. 2221-2295 (1916).

[17] S. Miyamoto, "A Theory on the Rate of Sublimation," *Trans. Faraday Soc.*, Vol. 29, pp. 794-797 (1933).

[18] Personal Communication, A. Majumdar, Thermal & Combustion Analysis Branch, NASA-Marshall Space Flight Center, Huntsville, AL (April 2015)